# MSEC2019-3034

# PREDICTING PART-LEVEL THERMAL HISTORY IN METAL ADDITIVE MANUFACTURING USING GRAPH THEORY: EXPERIMENTAL VALIDATION WITH DIRECTED ENERGY DEPOSITION OF TITANIUM ALLOY PARTS

Reza Yavari<sup>1</sup>, Jordan Severson<sup>1</sup>, Aniruddha Gaikwad<sup>1</sup>, Kevin Cole<sup>1\*</sup>, and Prahalada Rao<sup>1</sup>

<sup>1</sup>Mechanical and Materials Engineering, University of Nebraska-Lincoln, Lincoln, NE 68588-0526, United States

#### **ABSTRACT**

The objective of this paper is to experimentally validate the graph-based approach that was advanced in our previous work for predicting the heat flux in metal additive manufactured parts. We realize this objective in the specific context of the directed energy deposition (DED) additive manufacturing process. Accordingly, titanium alloy (Ti6Al4V) test parts (cubes) measuring 12.7 mm × 12.7 mm × 12.7 mm were deposited using an Optomec hybrid DED system at the University of Nebraska-Lincoln (UNL). A total of six test parts were manufactured under varying process settings of laser power, material flow rate, layer thickness, scan velocity, and dwell time between layers. During the build, the temperature profiles for these test parts were acquired using a single thermocouple affixed to the substrate (also Ti6Al4V). The graph-based approach was tailored to mimic the experimental DED process conditions. The results indicate that the temperature trends predicted from the graph theoretic approach closely match the experimental data; the mean absolute percentage error between the experimental and predicted temperature trends were in the range of 6% ~ 15%. This work thus lays the foundation for predicting distortion and the microstructure evolved in metal additive manufactured parts as a function of the heat flux. In our forthcoming research we will focus on validating the model in the context of the laser powder bed fusion process.

Keywords: Additive Manufacturing, Directed Energy Deposition, Thermal Modeling, Heat Flux Prediction, Graph Theory.

#### 1 Introduction

#### 1.1 Objective

Our previous work outlined the concept of heat diffusion over graphs and its application to thermal modeling in metal additive manufacturing processes [1]. This foregoing paper verified the heat flux trends predicted by the graph-based approach with those obtained using Goldak's moving heat source

finite element (FE) model simulations for three test part geometries [2, 3]. These test parts, which were simulated under laser powder bed fusion (LPBF) additive manufacturing process conditions, showed that the graph theoretic and FE-based approaches both converged to the same thermal trends; the symmetric mean absolute percentage error was less than 15%. More pertinently, the computation time required by the graph-based approach was significantly less than that required for a coarse mesh FE simulation – 4 minutes versus over 3 hours. Continuing with our previous research findings, the objective of this work is to experimentally validate the graph-based thermal modeling approach. We realize this objective in the specific context of the directed energy deposition (DED) metal additive manufacturing process in the context of Titanium alloy parts (Ti6Al4V).

#### 1.2 Motivation and Rationale

There are two challenges with obtaining heat flux measurements in LPBF that has motivated us to pursue experimental validation of the graph theory approach with DED in this work. The first challenge in experimental measurement of thermal trends in LPBF relates to the part being progressively buried within the powder as the layers are deposited, hence only the top surface of the part on the powder bed is exposed for thermal measurements [4]. Moreover, because the fixed LPBF substrate is so massive that thermocouples do not capture fine details of part temperature. While thermocouples can be embedded within the part by stopping the process, this will inevitably lead to altering the natural progress of the process [5]. Hence, researchers use thermal patterns at the meltpool and bedlevel as derived process signatures to validate thermal models for the LPBF process, typically, using a short wave infrared (SWIR) thermal camera [6-9].

The second challenge in obtaining thermal trends in LPBF is that, because, the thermal emissivity of the material varies as

<sup>\*</sup> Corresponding author. Email: Tel.: +01-402-472-5857. E-mail address: kcole1@unl.edu

it changes state from solid to liquid, and back to solid again, the thermal trends obtained using IR cameras are not absolute [10]. Moreover, the effect of image blur due to the high speed of the laser, obstruction due to the vapor generated during melting, and gas flow over the powder bed, among others, present significant obstacles to model validation in LPBF [11]. Alternatives to overcome this bottleneck are to: (1) use a dual wavelength pyrometer, (2) measure the part distortion using in-situ using strain gauges and compare the layer-by-layer part distortion with theoretically predicted heat flux trends as inputs into FE-based thermomechanical models [5], and (3) to estimate the residual stresses from the heat flux and validating the same with neutron diffraction or the slitting method [12, 13].

In contrast, in the DED process the part is not surrounded by powder and the DED substrate is much less massive than that for LPBF because the DED substrate translates on a 3-axis positioning system. Thus, the substrate temperature responds quite quickly to changes in the part temperature. The exposed nature of the part in DED lends to measurement of the heat flux using relatively inexpensive contact-based thermocouples embedded in the substrate [14]. In the forthcoming section we describe the experimental setup and the ensuing model validation results in the context of DED. We refer the reader to the pioneering works of Heigel *et al.* who have characterized the effect of DED process parameters on part distortion by devising novel in-situ measurement approaches based on linear displacement sensors [14, 15].

#### 2 Experimental Setup

### 2.1 Test Part and Sensing Setup

 $4 \text{ mm} \times 25.4 \text{ mm} \times 19.1 \text{ mm}$ , L×B×H) as shown in Figure 1(a). During the build, process temperature measurements were acquired with a K-type thermocouple (Omega WTK-14-144). As shown in Figure 1(b) the thermocouple is bolted onto a blind hole drilled and tapped on the side of the substrate. To mitigate measurement variation, the same thermocouple was used for all test parts. This was achieved by relocating the thermocouple to the vicinity of a new test part. The side-mounted arrangement makes it tractable for the operator to bolt-unbolt the thermocouple without having to dismount the entire substrate. We note that the DED machine was maintained under argon atmosphere, and the change in position of the thermocouple was performed through glove ports in the machine without change of ambient conditions. The thermocouple signals are conditioned through a National Instruments (NI) data acquisition system consisting of NI 9213 24-bit C-Series thermocouple data acquisition module integrated with a NI cDAO-9188 signal conditioning chassis, and subsequently processed in the Labview environment.

Limitations of the Experimental Setup: In its current form we acknowledge the following two limitations with our current experimental setup. First, by using a thermocouple with a bolting arrangement, the active junction of the thermocouple is inherently farther away from the point where the connection

(bolting) with the substrate is made. In other words, the location of measurement and attachment of the sensor are not the precisely the same. Since the temperature measurements are made farther away from the meltpool, and there is a possibility of an airgap between the substrate and the thermocouple, the thermal gradients observed in the thermal data are not considerably steep, i.e., the thermal gradients as observed are more gradual.

Secondly, the drilling of holes into the substrate inherently influences the heat transfer phenomena – the effect of holes in the substrate has not been accounted in the current work. Moreover, the holes drilled are not consistently at the same distance with respect to the part, whilst we have taken care to replicate the thermocouple position in our simulation studies, there is nonetheless a position-related error. To overcome these limitations, our forthcoming works will use a thermocouple arrangement that is spot welded onto the substrate, and positioned closer to the part as done in pioneering works reported in Ref. [14, 16].

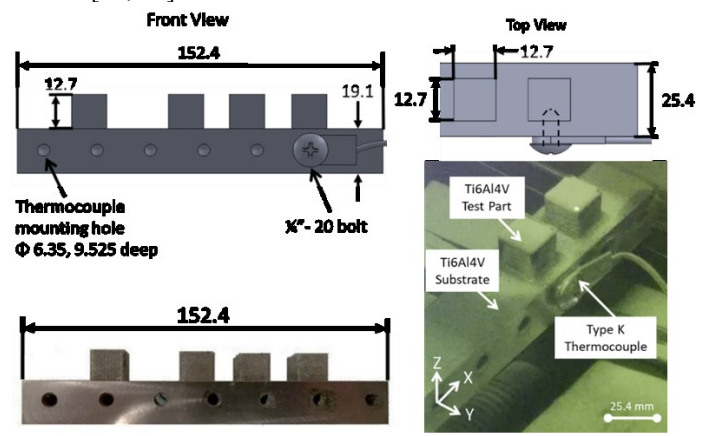


Figure 1: (a) The arrangement of the test parts on the substrate (152.4  $mm \times 25.4 mm \times 19.1 mm$ ), and dimensions thereof. (b) photograph of the actual implementation in the DED machine.

#### 2.2 Process Parameters

The process parameters used in the experiment are shown in Table 1. There are two broad parameter sets stratified by the laser power (475 W and 493 W), hatch spacing (0.75 mm and 0.305 mm), and deposition speed (630 mm/min and 1020 mm/min) settings. These parameter sets are accordingly labeled Case 1 and Case 2 respectively. Within both Case 1 and Case 2, the dwell time, i.e., the time the deposition of material halts between layers, is varied at three levels of 0 seconds, 20 seconds, and 40 seconds. Care was taken to ensure that an equilibrium with the build chamber ( $\approx$  25 °C) was reached between deposition of parts; a time gap of approximately 40 minutes was required for the temperature at the thermocouple location to attain equilibrium with the chamber.

The effect of dwell time manifests itself as prominent cyclical pattern between layers (Figure 5). The effect of dwell time on distortion and residual stress in DED is quantified by Denlinger et al. [17] who report the least distortion for 0-second

dwell time for Ti6Al4V in comparison to 40-second and 60-second dwell times. However, this trend is not evidenced in the case of Inconel 625. Previous research by Wang et al. reports the interdependence of process parameters, cooling rates, and the evolved microstructure in DED of thin wall parts [18].

A study by Yadollahi *et al.* substantiates the beneficial effect of longer dwell time (referred to as inter-layer intervals), as it leads to finer microstructures, uniform strength, and improved mechanical properties as a result of higher cooling rates [17]. The reader is also referred to the detailed two-part study by Yadollahi *et al.* that links process parameters, thermal behavior, microstructural evolution and properties of DED parts [17], as well as a comprehensive review articles by DebRoy *et al.* and Murr *et al.* on the process-structure-property relationships in metal additive manufacturing [18-20].

The process conditions in the current paper were selected for another much larger study focused on understanding

of process parameters, and heat flux on defect and microstructural evolution in DED as part of our future work. The hatch pattern used for all test parts was of the cross-type; this hatch pattern switches every layer so that the deposition direction for each layer is perpendicular to the layer that was deposited immediately before, i.e., the hatch angle alternates between  $0^{\circ}$  and  $90^{\circ}$ .

In closing this section we further note that, as reported in Table 1, the thermocouple sensor data is acquired at different sampling rates for roughly one-third of the duration of the experiment. For example, experimental data is available for 15 layers out of a total of 50 layers for Case 1 with 40-second dwell time. As we will present in Figure 5 in the forthcoming section, the process is observed to reach a steady state well within the duration for which the sensor data is available. The sampling characteristics of the thermocouple is varied to ascertain the optimal sampling frequency for future studies.

Table 1: Process parameters for experiment conducted by authors.

Case	Programmed Dwell Times [sec]	Power [W]	Powder Feed Rate [g/min]	Layer Thickness [mm]	Hatch Spacing [mm]	Deposition Speed [mm/min]	Total Number of Layers	Number of Layers Collected Data (Sensor Sampling Rate)	Experiment Duration [min]
1	0	475	4	0.254	0.75	630	50	20 (1 kHz)	17
	20							18 (10 Hz)	33
	40							15 (1 kHz)	49
2	0	493	3.3	0.457	0.305	1020	27	12 (1 kHz)	13
	20							9 (10 Hz)	22
	40							11 (10 Hz)	30

## 3 Procedure for Simulating the DED Process with Graph Theory Approach

#### 3.1 Model Assumptions

- The parameters used for the simulation and the material properties used in the simulation are shown in Table 2.
   The following assumptions are made to simplify the computational burden:
- The layer thickness and hatch spacing are aggregated into super-layers and super-hatches. Each super-layer consists of 2 individual layers of size 0.254 mm in Case 1 and 0.457 mm in Case 2. Each super hatch includes of 2 individual hatches of size 0.75 mm in Case 1 and 0.305 mm in Case 2. From the experimental perspective, data from two layers and hatches are likewise averaged.
- The simulation proceeds in terms of discrete material deposition steps divided into blocks (Figure 3). The material inside a block (length of 1.77 mm, breadth of 2 hatch thickness, and height of 2 layers) is considered to be deposited and melted instantaneously.
- The length of the substrate (i.e., the plate on which the parts are deposited) is scaled to 76.2 mm, i.e., half of its actual length of 152.4 mm, in turn, the need to simulate the heat flux for the entire substrate is avoided. The

- feasibility of this assumption is demonstrated by Williams et al. [21].
- Heat loss due to free convection is assumed to occur uniformly on all surfaces of the test part. The coefficient of convection, h<sub>w</sub>, is set to  $1 \times 10^{-6}$  (W/m<sup>2</sup>. K) per Ref. [20]. This assumption can be a major cause of estimation errors in the heat flux as demonstrated by Heigel et al., who have instead used a FE-model based on in-situ forced convection measurements to account for the flow of inert carrier gas from the nozzle on the part [14].
- Furthermore, as indicated in our previous manuscript, the simulated temperature values are obtained as normalized values between 0 and 1 [1]. Herein, we have linearly scaled the predicted temperature to the corresponding range of 298 K (25 °C) to 1873 K (1600 °C). The lower end corresponds to the ambient temperature of the build chamber, while the upper limit is the approximate melting point of Ti6Al4V. Pertinently, we note that apart from the neighborhood distance, material-related properties used for the graph theory simulation are identical to these in our previous work [1].

# 3.2 Simulation Procedure, Conditions, and Material Properties

The simulation procedure is schematically shown in Figure 2, and consists of the four steps in the graph theory approach delineated in our previous work. These are summarized here again. First, the part geometry is represented as discrete nodes. Second, the pairwise distance between nodes is calculated, and only those nodes whose standardized Gaussian distance is less than a certain threshold value (neighborhood distance,  $\epsilon$ ) are connected. Third, the deposition and powder melting process is simulated accounting for the hatch pattern and the deposition speed (scan velocity), and the heat is diffused across the preceding hatches and layers. The simulation proceeds in discrete steps of 0.2 second for Case 1, and 0.1 second for Case 2. Fourth, the process is continued until the part is built.

#### 4 Results

Representative results for the predicted thermal distribution are shown in qualitative terms in Figure 3. To explain further, in Figure 3, snapshots of the temperature distribution over the part at the end of super-layers 3, 6, and 9 for the three dwell times for

Case 2 are captured. The temperature distribution is discernably a function of the dwell time. We believe the lower maximum temperature at higher dwell time means that heat is able to uniformly spread through the substrate. The ripples in the temperature signals at higher dwell time also show the spreading effect. Furthermore, in Figure 5 the temperature trends gathered by the thermocouple embedded within the substrate are juxtaposed against those predicted using graph theory for the six test parts, and the errors therefrom are estimated in terms of the mean absolute percentage error (MAPE) [14]. In parts built with no dwell time between layers the temperature increases linearly, and thereafter reach a steady state. MAPE defined in Eqn. 1, is used to quantify the error, where t is the time step and e is the absolute error.

$$MAPE = \frac{100\%}{n} \sum_{\forall t} e(t)$$

$$e(t) = \frac{|\text{Experiment } (t) - \text{Graph Theoretic solution}(t)|}{\left(\text{Experiment } (t)\right)}$$
(1)

Table 2. Process Parameters for the Graph Theoretic Simulation

Downwortows	Values			
Parameters	Case 1	Case 2		
Super layer thickness (mm)	0.51 (2 layers)	0.91 (2 layers)		
Super hatch thickness (mm)	1.5 (2 hatches)	0.6 (2 hatches)		
Total number of nodes in the part	7905	8460		
Neighborhood Distance, $\epsilon$ , (mm)	4	4		
Node Density	5 nodes in 1.5 mm <sup>3</sup>	5 nodes in 1.08 mm <sup>3</sup>		
Simulation Time Step, t, (sec)	0.2	0.1		
Convection coefficient wall, h <sub>w</sub> (W/m <sup>2</sup> . K) [18]	1 × 10 <sup>-6</sup>			
Convection coefficient substrate (sink), h <sub>s</sub> (W/m <sup>2</sup> . K)	1 × 10 <sup>-2</sup>			
Thermal Diffusivity, α (m²/s)	7 × 10 <sup>-6</sup>			
Density, $\rho$ (kg/m <sup>3</sup> )	4,300			
Ambient Temperature, $T_{\infty}$ (K)	298			

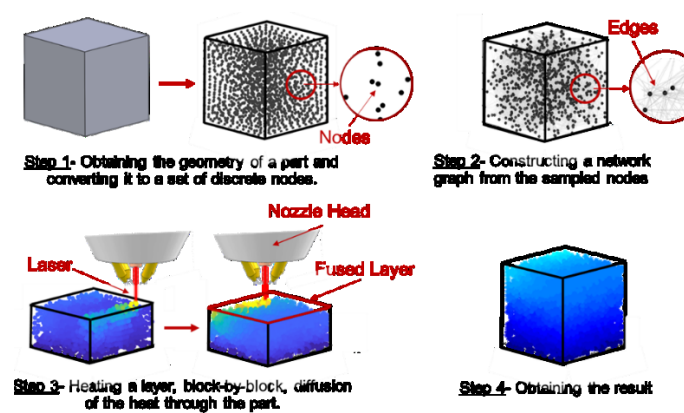


Figure 2. The four steps in the graph theoretic approach used to simulate the heat flux in the part hatch-by-hatch. Here we show an embodiment of the deposited energy deposition (DED) process.

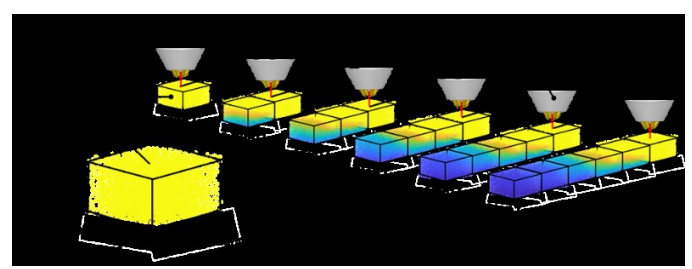


Figure 3. The simulation of discrete block-by-block simulation of the DED process. Each block consists of 2 layers, and 2 hatches, and the block length is 1.7 mm.

For the parts built with non-zero dwell times, each peak in the thermal profile corresponds to the end of a super-layer. Likewise, the time between the peak and trough corresponds to the end of the dwell cycle. Further, we note that barring the trends for Case 1, 20 second dwell time, the location of each super-layer evident in the cyclical pattern, and the amplitude of the oscillations are accurately imitated by the simulation.

In Case 1, 20 second dwell time (Figure 5 (a2)) a second small amplitude peak is noticed between each super-layer, i.e., there is a discrepancy in the cyclical pattern between layers. The source for this anomaly is hypothesized as a result of loose connection between the thermocouple and the substrate; the contact between the thermocouple and substrate was lost momentarily during translation of the table in the y-direction. There are two major reasons for the seemingly inconsistent variations in the measured experiment and simulation temperature values:

- The heat source in graph theoretic approach is applied as melting-temperature nodes instead of flux. The difference of heat source nature in simulation and experiment causes the larger values with the experiment when the laser is at the highest value (493 W) in Case 2.
- Since the sensor could be removed and placed at different locations using the gloves located in the front door of the DED, the contact/fit would be slightly different at each new location. This leads to changes in the rate of conduction.
- Different locations of the cube on the substrate (center versus near the free ends) causes a small difference in convection and conduction which affects the result.

Lastly, the mean absolute percentage error (MAPE) was estimated as indicator of goodness-of-fit between the predicted and measured heat flux trends; as reported in Table 3 these ranged between  $6\% \sim 15\%$ . The computation time ranged between 303 minutes to 337 minutes (approximately 5 hours) for the number of layers simulated.

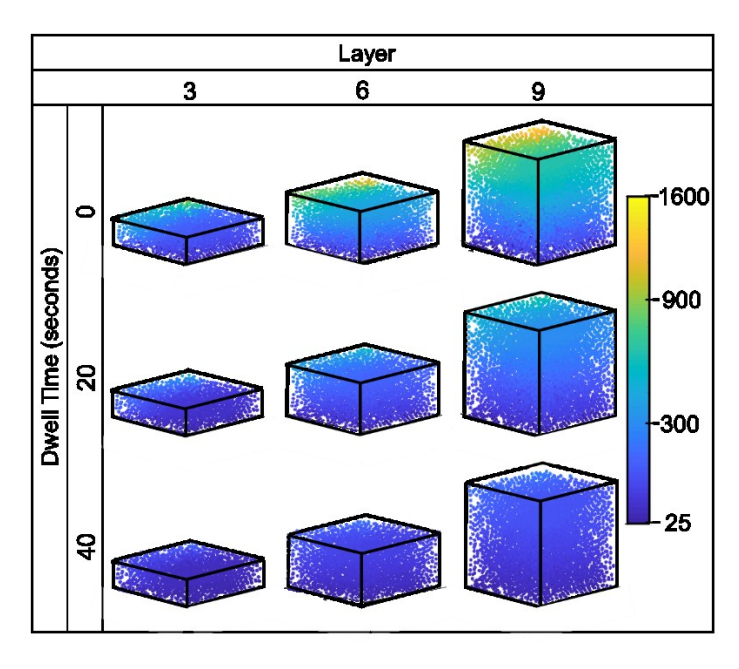


Figure 4.Temperature distribution snapshot captured after deposition process and dwell time for Case 2. The part is 12.7 mm  $\times$  12.7 mm in size.

#### 5 Conclusions and Future Work

This work reports the experimental validation of the graph-based approach presented in our previous manuscript for prediction of heat flux in the directed energy deposition (DED) metal additive manufacturing process in the specific context of directed energy deposition [1]. Heat flux trends during DED of six titanium alloy (Ti6Al4V) parts under varying process conditions were obtained using a thermocouple located on the substrate (also Ti6Al4V). The DED process conditions were emulated using the graph-based approach, and heat flux trends obtained therefrom were compared with the experimental trends; the mean absolute percentage error (MAPE) was in the range of  $6\% \sim 15\%$ .

This result thus supports the viability of using the graph theoretic approach in modeling of the heat flux in metal additive manufacturing. However, this result remains to be verified further in terms of more experimental data with improved apparatus and sensors, as well as for different processes, such as laser powder bed fusion. To take this work forward, we will address the following question foundational to part quality in metal AM in our forthcoming work: What is the effect of process conditions, part design (geometry), and material characteristics on the heat flux and consequently defects such as microstructure heterogeneity and distortion? In other words, we will endeavor to quantify the following link across a range of metal AM processes, such as powder bed fusion directed energy deposition:  $Process\ Parameters + Part\ Design\ + Material\ Characteristics \rightarrow Heat\ Flux \rightarrow Part\ Defects$ 

This knowledge is the key towards establishing a model-based closed-loop control approach to identify and correct defects in metal AM.

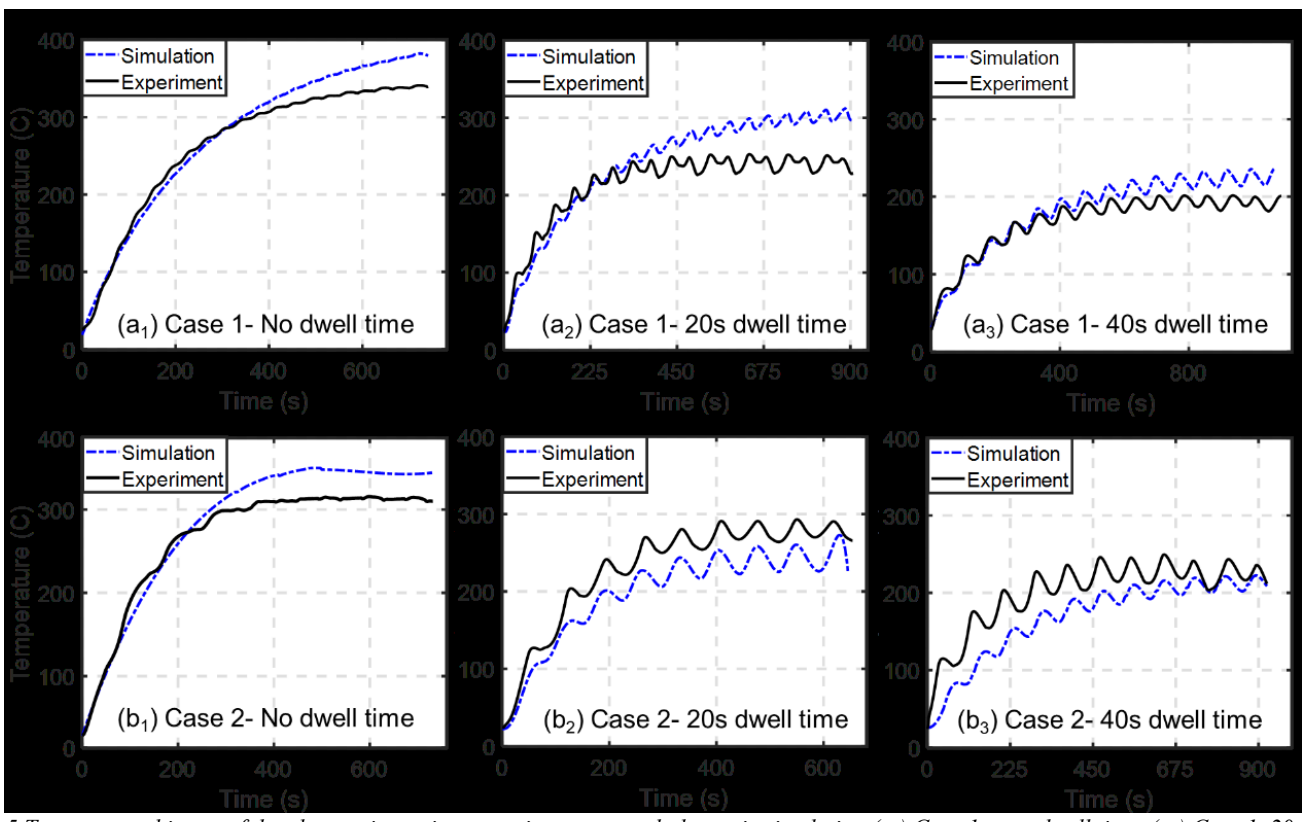


Figure 5.Temperature history of the observation points experiment vs graph theoretic simulation (a1) Case 1, zero dwell time, (a2) Case 1, 20 second dwell time, (a3) Case 1 40 second dwell time, (b1) Case 2, zero dwell time, (b2) Case 2, 20 second dwell time, and (b3) Case 2, 40 second dwell time.

Table 3. Comparison of Mean Absolute Percentage Error (MAPE) for the Graph Theoretic Simulation and Experiment for Case 1 and 2 shown in Figure 5.

	Dwell Time (sec)	MAPE	Computation Time (min)
	0	6.26%	303
Case 1	20	13.48%	309
	40	5.75%	312
	0	7.50%	330
Case 2	20	13.41%	333
	40	14.89%	337

#### **Acknowledgements**

One of the authors (PKR) thanks the NSF for funding his research through the following grants CMMI-1719388, CMMI-1739696 and CMMI-1752069 (CAREER) at University of Nebraska-Lincoln. Specifically, the concept of using graph theory for modeling in metal additive manufacturing applications was funded through CMMI-1752069 towards a correct-as-you-build smart additive manufacturing paradigm. The authors are grateful to Dr. Joseph Turner for permitting acquisition of thermocouple data during the DED builds intended for his NASA-funded research projects. The help of Mr. Grant King, Mr. Ben Bevans, Ms. Luz Sotelo, Mr. Cody Kanger, and Mr. Rakesh Karunakaran in obtaining the experimental data

is also gratefully acknowledged by the authors. Lastly, the authors express thanks to Dr. Abdalla Nassar, Applied Research Laboratory, Pennsylvania State University, for constructive discussions and suggestions to improve the experimental aspects of this work.

#### References

- [1] Yavari, R., Cole, K., and Rao, P., 2019, "A graph theoretic approach for near real-time prediction of part-level thermal history in metal additive manufacturing processes (Under Review, Submitted)," ASME Manufacturing Science and Engineering ConferenceErie, PA.
- [2] Goldak, J., Chakravarti, A., and Bibby, M., 1984, "A new finite element model for welding heat sources," Metallurgical Transactions B, 15(2), pp. 299-305.
- [3] Goldak, J. A., and Akhlaghi, M., 2005, "Computer simulation of welding processes," Computational Welding Mechanics, pp. 16-69.
- [4] Everton, S. K., Hirsch, M., Stravroulakis, P., Leach, R. K., and Clare, A. T., 2016, "Review of in-situ process monitoring and in-situ metrology for metal additive manufacturing," Materials & Design, 95, pp. 431-445.
- [5] Dunbar, A., Denlinger, E., Heigel, J., Michaleris, P., Guerrier, P., Martukanitz, R., and Simpson, T., 2016,

- "Development of experimental method for in situ distortion and temperature measurements during the laser powder bed fusion additive manufacturing process," Additive Manufacturing, 12, pp. 25-30.
- [6] Fox, J. C., Lane, B. M., and Yeung, H., "Measurement of process dynamics through coaxially aligned high speed near-infrared imaging in laser powder bed fusion additive manufacturing," Proc. Thermosense: Thermal Infrared Applications XXXIX, International Society for Optics and Photonics, p. 1021407.
- [7] Heigel, J. C., and Lane, B. M., 2018, "Measurement of the melt pool length during single scan tracks in a commercial laser powder bed fusion process," Journal of Manufacturing Science and Engineering, 140(5), p. 051012.
- [8] Lane, B., Mekhontsev, S., Grantham, S., Vlasea, M., Whiting, J., Yeung, H., Fox, J. C., Zarobila, C., Neira, J., and McGlauflin, M., "Design, developments, and results from the nist additive manufacturing metrology testbed (ammt)," Proc. Proceedings of the 26th Annual International Solid Freeform Fabrication Symposium—An Additive Manufacturing Conference, pp. 1145-1205.
- [9] Mani, M., Lane, B. M., Donmez, M. A., Feng, S. C., and Moylan, S. P., 2017, "A review on measurement science needs for real-time control of additive manufacturing metal powder bed fusion processes," International Journal of Production Research, 55(5), pp. 1400-1418.
- [10] Tapia, G., and Elwany, A., 2014, "A review on process monitoring and control in metal-based additive manufacturing," Journal of Manufacturing Science and Engineering, 136(6), p. 060801.
- [11] Huang, Y., Leu, M. C., Mazumder, J., and Donmez, A., 2015, "Additive Manufacturing: Current State, Future Potential, Gaps and Needs, and Recommendations," Transactions of the ASME, Journal of Manufacturing Science and Engineering, 137(1), p. 014001.
- [12] Wang, Z., Denlinger, E., Michaleris, P., Stoica, A. D., Ma, D., and Beese, A. M., 2017, "Residual stress mapping in Inconel 625 fabricated through additive manufacturing: Method for neutron diffraction measurements to validate thermomechanical model predictions," Materials & Design, 113, pp. 169-177.
- [13] Mercelis, P., and Kruth, J.-P., 2006, "Residual stresses in selective laser sintering and selective laser melting," Rapid prototyping journal, 12(5), pp. 254-265.
- [14] Heigel, J., Michaleris, P., and Reutzel, E., 2015, "Thermomechanical model development and validation of directed energy deposition additive manufacturing of Ti–6Al–4V," Additive manufacturing, 5, pp. 9-19.
- [15] Heigel, J. C., Michaleris, P., and Palmer, T. A., 2015, "In situ monitoring and characterization of distortion during laser cladding of Inconel® 625," Journal of Materials Processing Technology, 220, pp. 135-145.
- [16] Corbin, D. J., Nassar, A. R., Reutzel, E. W., Beese, A. M., and Michaleris, P., 2018, "Effect of Substrate Thickness and

- Preheating on the Distortion of Laser Deposited Ti-6Al-4V," Journal of Manufacturing Science and Engineering, 140(6), pp. 061009-061009-061009.
- [17] Shamsaei, N., Yadollahi, A., Bian, L., and Thompson, S. M., 2015, "An overview of Direct Laser Deposition for additive manufacturing; Part II: Mechanical behavior, process parameter optimization and control," Additive Manufacturing, 8, pp. 12-35.
- [18] DebRoy, T., Wei, H. L., Zuback, J. S., Mukherjee, T., Elmer, J. W., Milewski, J. O., Beese, A. M., Wilson-Heid, A., De, A., and Zhang, W., 2018, "Additive manufacturing of metallic components Process, structure and properties," Progress in Materials Science, 92, pp. 112-224.
- [19] Murr, L., 2018, "A metallographic review of 3D printing/additive manufacturing of metal and alloy products and components," Metallography, Microstructure, and Analysis, pp. 1-30.
- [20] Murr, L. E., Gaytan, S. M., Ramirez, D. A., Martinez, E., Hernandez, J., Amato, K. N., Shindo, P. W., Medina, F. R., and Wicker, R. B., 2012, "Metal fabrication by additive manufacturing using laser and electron beam melting technologies," Journal of Materials Science & Technology, 28(1), pp. 1-14.
- [21] Williams, R. J., Davies, C. M., and Hooper, P. A., 2018, "A Pragmatic Part Scale Model for Residual Stress and Distortion Predictionin Powder Bed Fusion," Additive Manufacturing.